Effect of Ca substitution on crystal structure and band gap of solar cell material $BaSi_2$

Motoharu Imai[a]* and Yoshitaka Matsushita[b]
[a]Research Center for Electrical and Optical Materials, National Institute for Materials Science, Ibaraki 305-0047, Japan
[b]Research Network and Facility Services Division, National Institute for Materials Science, Ibaraki 305-0047, Japan

E-mail: MATSUSHITA.Yoshitaka@nims.go.jp (Y. Matsushita)

*Corresponding author
Motoharu Imai
National Institute for Materials Science, Ibaraki 305-0047, Japan
Phone number:
E-mail: IMAI.Motoharu@nims.go.jp

Abstract
To ameliorate the potential of a promising solar cell material $BaSi_2$, the effects of substituting Ba with Ca atoms on the crystal structure and band gap E_g of $BaSi_2$, were investigated both experimentally and computationally. The solid-solution limit of the Ca atoms in $BaSi_2$ was approximately 2.3 at.%. Single-crystal X-ray diffraction analysis of $Ba_{1-x}Ca_xSi_2$ ($0.025 \leq x \leq 0.072$) revealed that the unit cell volume decreases with Ca content x, and the Ba atoms at the A1 crystallographic site are preferentially substituted by Ca atoms. Diffuse reflectance measurements indicated that E_g decreases with x (1.24 eV at $x = 0$ and 1.17 eV at $x = 0.07$). The density functional theory calculations demonstrate that the experimentally observed decrease in E_g by Ca substitution can be explained qualitatively by the combination of the substitution of Ca atoms in the unit cell volume of $BaSi_2$ and the volume reduction.

Keywords
Silicides, Semiconductors, Crystal structure, Optical properties, Electronic structure

ORCID ID
M. Imai: 0000-0002-5848-113X
Y. Matsushita: 0000-0002-4968-8905

1. Introduction

Barium disilicide ($BaSi_2$), which is composed only of earth-abundant elements, has been investigated as a suitable candidate for next-generation thin-film solar cells [1-8] owing to its promising properties as a photoabsorber. $BaSi_2$ has a band gap (E_g) of 1.1–1.3 eV, a large absorption coefficient at 1.5 eV (>10^4 cm^{-1}), high quantum efficiency (>70%), long minority-carrier lifetime (11–14 μs), and long diffusion length for minority carriers [2, 3]. A $BaSi_2$ homojunction diode with a thickness of 2 μm was simulated to achieve a convergent efficiency of 25% [2]. Recent experiments have demonstrated that $BaSi_2$/n-Si solar cells have a conversion efficiency of approximately 9–10% [7, 8].

To broaden the potential of $BaSi_2$ as a solar cell material, investigating band gap tuning by substitution is important. The effects of Sr substitution on the crystal structure and E_g of $BaSi_2$ were examined computationally and experimentally [9-11]. $BaSi_2$ crystallizes into a unique crystal structure with Si_4 tetrahedra, the $BaSi_2$-type, which has two crystallographic sites for the Ba atoms and three for the Si atoms [12], as shown in Fig. 1 (a). Consequently, two possible substitution sites for the Ba atoms (A1 and A2) and three sites for the Si atoms (Si1, Si2, and Si3) exist. The local environments of the A1 and A2 sites are different; the Ba atoms at the A1 site have 9 Si atoms as neighbors, whereas the A2 site has 11 Si atoms as nearest neighbors. Single-crystal X-ray diffraction (XRD) and diffuse reflectance measurements of $Ba_{1-x}Sr_xSi_2$ ($0.0 \leq x \leq 0.8$) revealed that the Ba atoms at the A1 site are preferentially substituted by Sr atoms, and E_g decreases with x (1.24 eV at $x = 0$ and 1.15 eV at $x = 0.65$) [11]. The preferential occupation of the A1 site by Sr atoms is consistent with the computational result for $Ba_{0.5}Sr_{0.5}Si_2$, wherein, Ba atoms at the A1 site substituted with Sr are more stable than those in which Ba atoms at the A2 site substituted with Sr [10,11].

However, the effects of substitution with other elements have not yet been investigated. Although the pseudo-binary system of $BaSi_2$ and $CaSi_2$ has been reported to exhibit a eutectic phase diagram [13], no other experimental studies on ternary Ba–Ca silicides have been reported.

In this study, we investigated the effect of Ca substitution on the crystal structure and band gap of $BaSi_2$. We synthesized Ca-substituted $BaSi_2$, $Ba_{1-x}Ca_xSi_2$, determined their crystal structures, and estimated their band gaps using diffuse reflectance measurements. In addition, we determined the band structure of $Ba_7Ca_1Si_{16}$ using density functional theory (DFT) calculations. Finally, the experimental and computational results are compared and discussed.

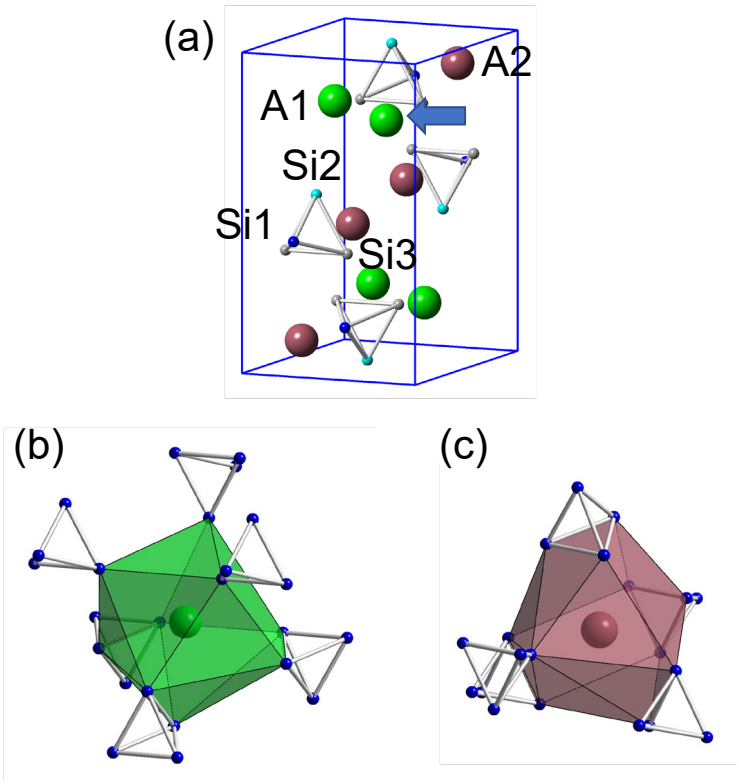

Fig. 1. (a) Crystal structure of $BaSi_2$ [11]. Green, red, blue, sky-blue, and gray spheres represent atoms at A1, A2, Si1, Si2, and Si3 sites, respectively. The arrow indicates a Ba atom replaced by a Ca atom in the electronic structure calculation of $Ba_7Ca_1Si_{16}$. Coordination polyhedra at (b) the A1 and (c) A2 sites.

2. Experimental and computational methods

$BaSi_2$ and $CaSi_2$ were synthesized by Ar-arc melting a 1.03:2 molar mixture of Ba (or Ca) and Si. The $Ba_{1-x}Ca_xSi_2$ samples were prepared in two steps: Ar-arc melting of a mixture of $BaSi_2$ and $CaSi_2$, followed by remelting and slow cooling of arc-melted $Ba_{1-x}Ca_xSi_2$ and subsequent annealing. A $(1-x_s):x_s$ molar mixture of $BaSi_2$ and $CaSi_2$ (x_s = 0.05, 0.10, 0.15, 0.16, and 0.20) was Ar-arc melted. The resultant ingot loaded into a BN crucible was melted in an Ar atmosphere by heating at 1470 K for 2 h, cooling to 1140 K at 5 K/h, and maintaining at 1140 K for 24 h. The detailed synthesis procedure is described in a previous study [11]. Prior to this melting step, the melting temperature of the arc-melted ingots was confirmed to be less than 1470 K using differential thermal analysis. The chemical composition of the samples was evaluated by electron probe microanalysis (EPMA). The details of the preparation method for the EPMA samples are described in a previous study [14].

The structures of single crystals isolated from the samples were determined using the XRD technique, which was performed using a four-axes goniometer equipped with a charge-coupled device area detector (Rigaku, AFC11 and Saturn 724+, graphite-monochromated Mo-Kα radiation, λ = 0.71073 Å) at room temperature. The following software programs were used for the XRD analysis: CrystalClear [15] for data collection, cell refinement, and data reduction, and SHELXL-97 [16] for structure refinement.

Diffuse reflectance spectra were recorded in the range of 190–2000 nm using a spectrometer (JASCO Co. V-570) equipped with an integrating sphere attachment. Optical absorbance spectra were obtained by converting the diffuse reflectance spectra using the Kubelka–Munk equation: $\alpha/S = (1-R)^2/2R$, where α, R, and S are the optical absorption coefficient, relative diffuse reflectance of a sample to the standard material, and scattering coefficient, respectively [17].

The band structure was calculated within the generalized gradient approximation of Perdew, Burke, and Ernzerhof (GGA- PBE) [18] using the Advance/PHASE program package [19]. A norm-conserving pseudopotential was employed for the Si atoms and an ultrasoft pseudopotential was utilized for the Ca and Ba atoms. The cut-off energies for plane waves and charge densities were 16.25 and 146.25 Hartree, respectively. A 4 × 4 × 2 Monkhorst–Pack k-point grid was adopted for convergence.

3. Results and discussion

3.1 Phase identification

Figure 2 shows backscattered electron images of the samples with x_s = 0.05, 0.10, and 0.15. The sample with x_s = 0.05 consists of a single phase (light gray area), while those with x_s = 0.10 and 0.15 consist of two phases (light and dark gray areas). The EPMA revealed that the light gray area corresponds to $Ba_{1-x}Ca_xSi_2$ (x = 0.04 and 0.05), and the dark gray area corresponds to $Ca_{1-y}Ba_ySi_2$ (y = 0.006 and 0.01). Figure 3 shows the Ca content of the light gray area determined by EPMA (x) as a function of x_s. x increases with x_s; however, x is smaller than x_s. x reaches 0.07 approximately at x_s = 0.20. x of 0.07 corresponds to 2.3 at.%. These results suggest that the $BaSi_2$–$CaSi_2$ pseudo-binary diagram has a eutectic phase, as suggested in a previous study [13], and the solid-solution limit of Ca in $BaSi_2$ is approximately 2.3 at.%, and that of Ba in $CaSi_2$ is approximately 0.4 at.%.

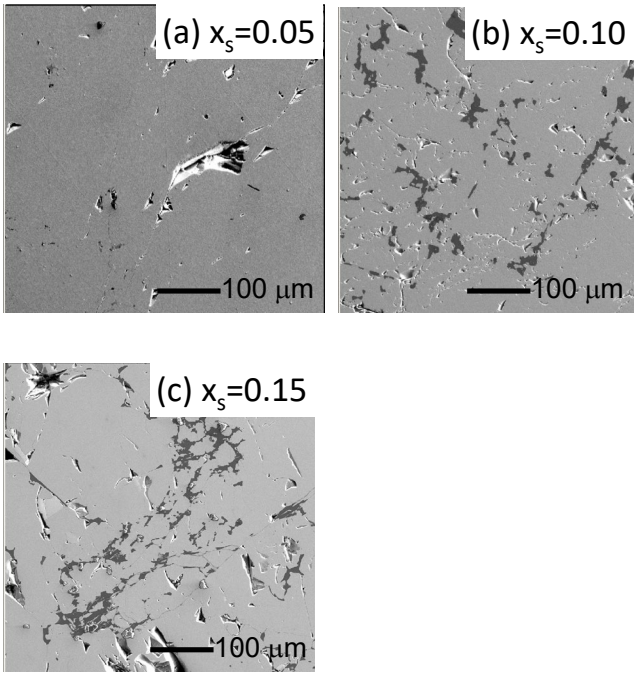

Fig. 2 Backscattered electron images of samples $Ba_{1-xs}Ca_{xs}Si_2$ with (a) x_s = 0.05, (b) x_s = 0.10, and (c) x_s = 0.15.

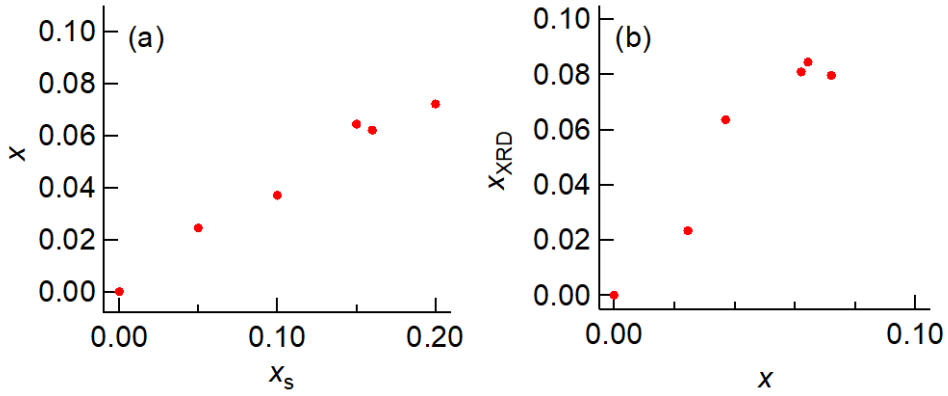

Fig. 3. (a) Ca content of $Ba_{1-xs}Ca_{xs}Si_2$ determined by EPMA (x) as a function of Ca content in the starting material (x_s). (b) Ca content of $Ba_{1-x}Ca_xSi_2$ determined by single-crystal XRD (x_{XRD}) as a function of x.

3.2 Crystal structure

Table 1 lists lattice parameters, atomic coordinates, and temperature factors of $Ba_{1-x}Ca_xSi_2$ determined by the single-crystal XRD measurements. Figure 4 (a) shows the lattice parameters normalized with those of $BaSi_2$ [20] as functions of the Ca content, x. The lattice parameters decrease monotonically with x, with the a/a_0 parameter decreasing slightly more than the other two, b/b_0 and c/c_0. The normalized lattice parameters of $Ba_{1-x}Ca_xSi_2$ are smaller than those of $Ba_{1-x}Sr_xSi_2$ for all the substitution element content.

The XRD analysis revealed that Ca atoms preferentially occupied only the A1 site for all x values. As shown in Fig. 4 (b), the occupancy of the A1 site increases with x. The x dependence of the Ca occupancy at the A1 site in $Ba_{1-x}Ca_xSi_2$ is almost the same as that of the Sr occupancy at the A1 site in $Ba_{1-x}Sr_xSi_2$. The preferential occupation of the A1 site by Ca atoms is consistent with the previously reported computational result for $Ba_{0.5}Ca_{0.5}Si_2$, wherein, the Ba atoms substituted with Ca at the A1 site are more stable than those of the Ba atoms substituted with Ca at the A2 site [10]. Figure 3 (b) shows the Ca content calculated based on the Ca occupancy determined from single-crystal XRD data (x_{XRD}) as a function of x. The x_{XRD} value is consistent with that of x, although the x_{XRD} value is slightly larger than that of x.

Figure 4 (c) shows the volumes of the coordination polyhedra at the A1 and A2 sites, Si_4 tetrahedron, and unit cell of $Ba_{1-x}Ca_xSi_2$ normalized with respect to those of $BaSi_2$ [20] as functions of x. The coordination polyhedra at the A1 and A2 sites are denoted as CP-A1 and CP-A2, respectively. The volume of CP-A2 (89.013 $Å^3$ for $BaSi_2$) is larger than that of CP-A1 (75.311 $Å^3$ for $BaSi_2$). All normalized volumes decreased

with increasing *x*, although the decrease in the Si_4 tetrahedron was smaller than that of the other three, unit cell, CP-A1, and CP-A2. The small decrease in the Si_4 volume is attributed to the covalent bonds forming the Si_4 tetrahedron [21,22]. For any given Ca content, the normalized volume of CP-A2 was larger than that of the unit cell, whereas that of CP-A1 was smaller than that of the unit cell. This result suggests that the volume of CP-A1 decreased more rapidly with an increase in Ca content than that of CP-A2.

Table. 1. Lattice parameters, atomic coordinates, and temperature factors (in Å^2) of $Ba_{1-x}Ca_xSi_2$ (orthorhombic, space group: *P*nma, No. 62, $Z = 8$). U_{eq} and U_{ij} (i, j = 1, 2, and 3) are the isotropic and anisotropic temperature factors, respectively. The values in the parenthesis are standard deviations.

(a) $x = 0.025$

Lattice parameters: $a = 8.9070(2)$ Å, $b = 6.7136(2)$ Å, $c = 11.5147(2)$ Å, $V = 688.56(3)$ Å^3. Final R indexes: $R_{int} = 0.0301$, $R\ [F^2 > 2\sigma(F^2)] = 0.0230$, $wR(F^2) = 0.0517$, $S = 1.193$.

Atomic site	Wyckoff position	*x*	*y*	*z*	Occupancy	U_{eq}
A1	*4c*	0.01435(2)	1/4	0.69337(2)	0.9533(12) Ba 0.0467(12) Ca	0.01332(3)
A2	*4c*	0.83853(2)	1/4	0.09466(2)	1 Ba	0.01479(3)
Si1	*4c*	0.41738(6)	1/4	0.08966(5)	1	0.01756(10)
Si2	*4c*	0.19714(6)	1/4	0.96526(4)	1	0.01487(9)
Si3	*8d*	0.19434(4)	0.42822(6)	0.14504(3)	1	0.01587(7)

Atomic site	U_{11}	U_{22}	U_{33}	U_{12}	U_{13}	U_{23}
A1	0.01255(4)	0.01422(6)	0.01319(4)	0.0000	-0.00033(2)	0.0000
A2	0.01715(5)	0.01312(6)	0.01411(4)	0.0000	0.00023(3)	0.0000
Si1	0.01277(18)	0.0227(3)	0.0172(2)	0.0000	0.00016(15)	0.0000
Si2	0.01696(19)	0.0163(2)	0.01136(16)	0.0000	-0.00123(14)	0.0000
Si3	0.01844(14)	0.01342(17)	0.01574(13)	0.00133(12)	-0.00028(11)	-0.00269(11)

(b) $x = 0.037$

Lattice parameters: $a = 8.8737(2)$ Å, $b = 6.70000(10)$ Å, $c = 11.4855(3)$ Å, $V = 682.86(3)$ Å^3. Final R indexes: $R_{int} = 0.0272$, $R\ [F^2 > 2\sigma(F^2)] = 0.0244$, $wR(F^2) = 0.0542$, $S = 1.315$.

Atomic site	Wyckoff position	*x*	*y*	*z*	Occ.	U_{eq}
A1	*4c*	0.01386(2)	1/4	0.69391(2)	0.8727(10) Ba 0.1273(10) Ca	0.01312(3)
A2	*4c*	0.83836(2)	1/4	0.09458(2)	1 Ba	0.01450(3)
Si1	*4c*	0.41913(6)	1/4	0.08909(4)	1	0.01853(8)
Si2	*4c*	0.19738(5)	1/4	0.96483(4)	1	0.01500(7)
Si3	*8d*	0.19530(4)	0.42875(5)	0.14504(3)	1	0.01637(6)

Atomic site	U_{11}	U_{22}	U_{33}	U_{12}	U_{13}	U_{23}
A1	0.01236(4)	0.01385(4)	0.01313(4)	0.0000	-0.00051(2)	0.0000
A2	0.01710(5)	0.01259(4)	0.01379(4)	0.0000	0.00026(2)	0.0000
Si1	0.01348(18)	0.0232(2)	0.01887(19)	0.0000	-0.00098(13)	0.0000
Si2	0.01732(17)	0.01567(16)	0.01201(15)	0.0000	-0.00175(13)	0.0000
Si3	0.01969(13)	0.01335(11)	0.01606(13)	0.00155(9)	-0.00103(10)	-0.00263(9)

(c) $x = 0.062$

Lattice parameters: $a = 8.8563(2)$ Å, $b = 6.6895(2)$ Å, $c = 11.4728(3)$ Å, $V = 679.70(3)$ Å^3. Final R indexes : $R_{int} = 0.0341$ R [$F^2 > 2\sigma(F^2)$] = 0.0284, w$R(F^2) = 0.0609$, $S =$ 1.369.

Atomic site	Wyckoff position	x	y	z	Occ.	U_{eq}
A1	*4c*	0.01362(2)	1/4	0.69413(2)	0.8381(12) Ba 0.1619(12) Ca	0.01295(4)
A2	*4c*	0.83832(2)	1/4	0.09456(2)	1 Ba	0.01425(3)
Si1	*4c*	0.41976(6)	1/4	0.08876(5)	1	0.01900(10)
Si2	*4c*	0.19752(6)	1/4	0.96470(4)	1	0.01511(8)
Si3	*8d*	0.19571(4)	0.42896(6)	0.14504(3)	1	0.01653(6)

Atomic site	U_{11}	U_{22}	U_{33}	U_{12}	U_{13}	U_{23}
A1	0.01215(5)	0.01369(5)	0.01301(5)	0.0000	-0.00054(2)	0.0000
A2	0.01689(5)	0.01232(5)	0.01355(5)	0.0000	0.00031(2)	0.0000
Si1	0.01412(18)	0.0236(3)	0.0192(2)	0.0000	-0.00154(15)	0.0000
Si2	0.01755(18)	0.0155(2)	0.01225(16)	0.0000	-0.00218(14)	0.0000
Si3	0.02002(14)	0.01340(14)	0.01619(14)	0.00148(10)	-0.00119(11)	-0.0261(10)

(d) $x = 0.064$

Lattice parameters: $a = 8.8529(2)$ Å, $b = 6.6874(2)$ Å, $c = 11.4654(3)$ Å, $V = 678.78(3)$ Å^3. Final R indexes: $R_{int} = 0.0355$ R [$F^2 > 2\sigma(F^2)$] = 0.0389, w$R(F^2) = 0.0725$, $S = 1.288$.

Atomic site	Wyckoff position	x	y	z	Occ.	U_{eq}
A1	*4c*	0.01353(2)	1/4	0.69423(2)	0.831(2) Ba 0.169(2) Ca	0.01285(5)
A2	*4c*	0.83830(2)	1/4	0.09455(2)	1 Ba	0.01421(5)
Si1	*4c*	0.41989(11)	1/4	0.08856(9)	1	0.01905(18)
Si2	*4c*	0.19763(11)	1/4	0.96453(8)	1	0.01501(15)

Si3	*8d*	0.19595(8)	0.42895(10)	0.14507(6)	1	0.01669(12)

Atomic site	U_{11}	U_{22}	U_{33}	U_{12}	U_{13}	U_{23}
A1	0.01191(7)	0.01361(9)	0.01303(8)	0.0000	-0.00055(5)	0.0000
A2	0.01678(8)	0.01226(8)	0.01360(8)	0.0000	0.00035(5)	0.0000
Si1	0.0139(3)	0.0237(5)	0.0195(4)	0.0000	-0.0017(3)	0.0000
Si2	0.0175(3)	0.0152(4)	0.0124(3)	0.0000	-0.0019(3)	0.0000
Si3	0.0200(3)	0.0135(3)	0.0166(3)	0.0015(2)	-0.0015(2)	-0.0027(2)

(e) $x = 0.072$

Lattice parameters: $a = 8.8624(4)$ Å, $b = 6.6934(3)$ Å, $c = 11.4723(6)$ Å, $V = 680.53(6)$ Å^3. Final R indexes: $R_{int} = 0.0365$, $R\ [F^2 > 2\sigma(F^2)] = 0.0224$, $wR(F^2) = 0.0527$, $S = 1.159$.

Atomic site	Wyckoff position	*x*	*y*	*z*	Occ.	U_{eq}
A1	*4c*	0.01366(2)	1/4	0.69411(2)	0.8406(10) Ba 0.1594(10) Ca	0.01374(3)
A2	*4c*	0.83834(2)	1/4	0.09455(2)	1 Ba	0.01509(3)
Si1	*4c*	0.41975(6)	1/4	0.08875(5)	1	0.01973(9)
Si2	*4c*	0.19748(6)	1/4	0.96465(4)	1	0.01590(8)
Si3	*8d*	0.19572(4)	0.42896(5)	0.14503(3)	1	0.01740(6)

Atomic site	U_{11}	U_{22}	U_{33}	U_{12}	U_{13}	U_{23}
A1	0.01323(5)	0.01413(4)	0.01385(5)	0.0000	-0.00053(3)	0.0000
A2	0.01803(5)	0.01286(4)	0.01439(5)	0.0000	0.00029(2)	0.0000
Si1	0.01497(19)	0.0240(2)	0.0202(2)	0.0000	-0.00128(15)	0.0000
Si2	0.01847(19)	0.01585(16)	0.01337(17)	0.0000	-0.00202(15)	0.0000
Si3	0.02123(14)	0.01396(12)	0.01701(14)	0.00143(10)	-0.00145(11)	-0.00253(9)

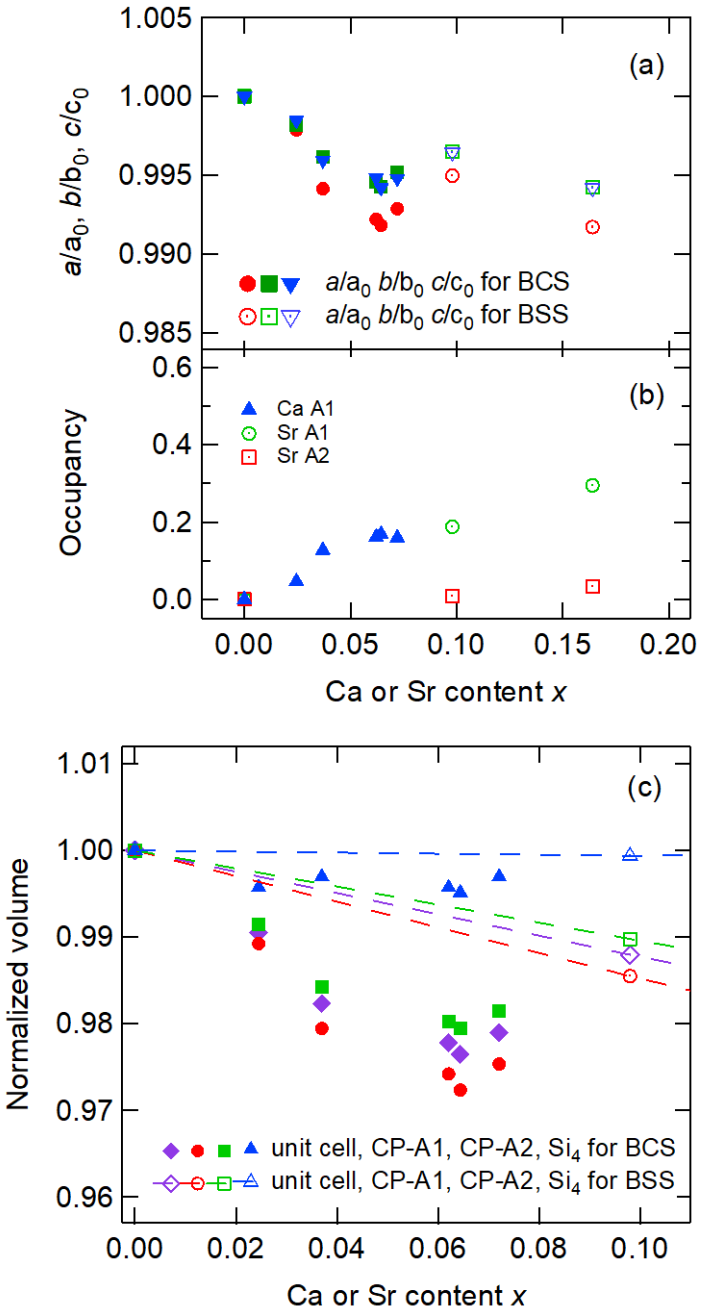

Fig. 4. (a) Lattice parameters normalized with respect to those of $BaSi_2$ [20] as functions of substitution element content (x). (b) Site occupancy of substitution atoms at A1 and A2 sites as a function of x. (c) Volumes of CP-A1, CP-A2, Si_4 tetrahedron, and unit cell normalized with respect to those of $BaSi_2$ [20], as functions of x. Solid and empty symbols represent data of $Ba_{1-x}Ca_xSi_2$ (BCS) and $Ba_{1-x}Sr_xSi_2$ (BSS), respectively.

3.3 Band gap

Figure 5 (a) shows the plot of the optical absorbance(α/S) of $Ba_{1-x}Sr_xSi_2$ as a function of the photon energy ($h\nu$), where α and S are the optical absorption coefficient and scattering coefficient, respectively. We defined the band gap (E_g) as the energy at which the extrapolated α/S curve intersects the extrapolation of the background (arrows in the figure), as proposed in a previous study [23].

Figure 5 (b) shows the E_g value of $Ba_{1-x}Ca_xSi_2$ obtained from α/S as a function of x. The E_g value of $BaSi_2$ is 1.24 eV, and E_g decreases with increasing x. The E_g values of $Ba_{1-x}Ca_xSi_2$ are smaller than those of $Ba_{1-x}Sr_xSi_2$ for all the substitution element content. The E_g value of $Ba_{1-x}Ca_xSi_2$ is 1.17 eV at x = 0.072, which corresponds to that of $Ba_{1-x}Sr_xSi_2$ at x = 0.58 (1.17 eV).

The lattice parameters of $Ba_{1-x}Ca_xSi_2$ at x = 0.072 were approximately the same as those of $Ba_{1-x}Sr_xSi_2$ at x = 0.16, and the E_g values of $Ba_{1-x}Ca_xSi_2$ at x = 0.072 were approximately similar to those of $Ba_{1-x}Sr_xSi_2$ at x = 0.58. This suggests that Ca substitution can decrease the E_g value with a smaller lattice deformation than Sr substitution.

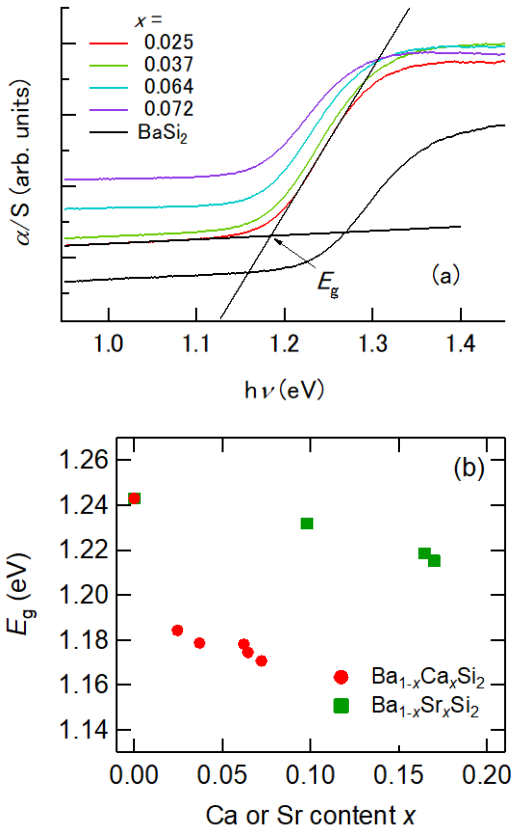

Fig. 5. (a) Optical absorbance (α/S) of $Ba_{1-x}Ca_xSi_2$ as a function of photon energy ($h\nu$). (b) Band gaps (E_g)of $Ba_{1-x}Ca_xSi_2$ and $Ba_{1-x}Sr_xSi_2$ [11] as functions of substitution element content (x). Red circles and green squares represent data of $Ba_{1-x}Ca_xSi_2$ and $Ba_{1-x}Sr_xSi_2$, respectively.

3.4 Calculated band structures

Band structures of the following six models were calculated: (a) $BaSi_2$ (Ba_8Si_{16}) with lattice parameters and atomic positions reported in Ref. 20; (b) $BaSi_2$ with lattice parameters and atomic positions of $Ba_{1-x}Ca_xSi_2$ with $x = 0.062$; (c) $Ba_7Ca_1Si_{16}$ with lattice parameters and atomic positions of $BaSi_2$ reported in Ref. 20; (d) $Ba_7Ca_1Si_{16}$ with lattice parameters and atomic positions of $Ba_{1-x}Ca_xSi_2$ with $x = 0.062$; (e) $Ba_7Sr_1Si_{16}$ with lattice parameters and atomic positions of $BaSi_2$ reported in Ref. 20; and (f) $Ba_7Sr_1Si_{16}$ with lattice parameters and atomic positions of $Ba_{1-x}Sr_xSi_2$ with $x = 0.10$ [11]. To create models (c) and (d), a Ba atom occupying the A1 site was replaced by a Ca atom in models (a) and (b). $BaSi_2$ has four Ba atoms at the A1 sites in its unit cell. We calculated the total energy of $Ba_7Ca_1Si_{16}$ with four different Ca atomic positions and confirmed that the total energies of the four models were the same within a convergence criterion of 1.0×10^{-9} Hartree. Thus, we demonstrate the band structure of $Ba_7Ca_1Si_{16}$ in which the Ba atom at the A1 site (marked by an arrow in Fig. 1) is replaced by a Ca atom. We created models (e) and (f) by replacing the Ba atom at the A1 site (marked by an arrow in Fig. 1) with a Sr atom. Figure 6 shows the band structures of $BaSi_2$ and $Ba_7Ca_1Si_{16}$. The volume of $Ba_7Ca_1Si_{46}$ is 0.982 V_0, where V_0 is the unit cell volume of $BaSi_2$. Figure 6 (a) revealed that $BaSi_2$ with $V = V_0$ is an indirect band gap semiconductor that has a valence band maximum (VBM) at the k-point between Γ and Y point and a conduction band minimum (CBM) at the T point, which is consistent with the previously reported results [5,6,10,11,24]. The remaining five, including $Ba_7Sr_1Si_{46}$, are also indirect band gap semiconductors with a VBM and CBM at the same k-points.

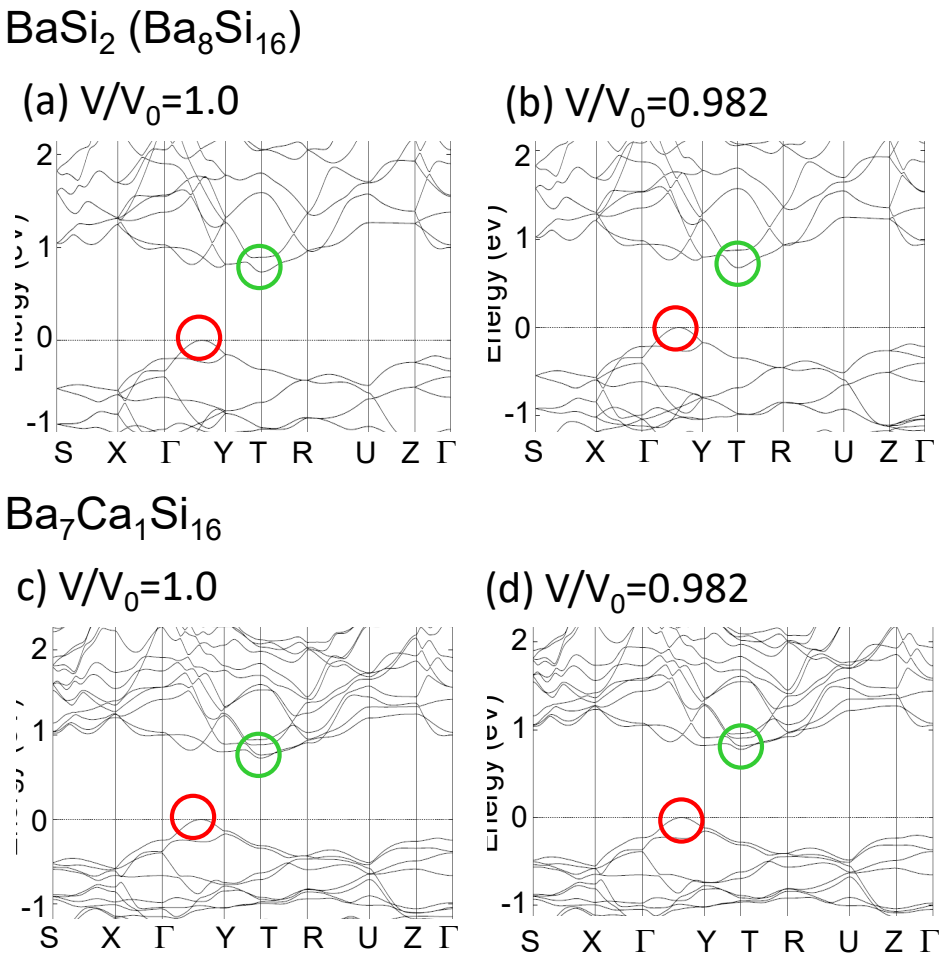

Fig. 6. Band structure of (a) $BaSi_2$ at $V/V_0 = 1.00$, (b) $BaSi_2$ at $V/V_0 = 0.982$, (c) $Ba_7Ca_1Si_{16}$ at $V/V_0 = 1.00$, and (d) $Ba_7Ca_1Si_{16}$ at $V/V_0 = 0.982$, where V and V_0 are the unit cell volume and unit cell volume of $BaSi_2$ at 0 GPa, respectively [20]. Red and green circles represent a valence band maximum and conduction band minimum, respectively.

3.5 Comparison of experimental and calculated band gap results

DFT calculations using GGA-PBE underestimate the band gap of semiconductors. Therefore, we calculated the difference in E_g between substituted $BaSi_2$ and $BaSi_2$, $\Delta E_g = E_g(V/V_0) - E_{g0}$ for both experimental and computational results and compared them, where E_{g0} is the band gap of $BaSi_2$ at $V = V_0$. Figure 7 shows ΔE_g for $Ba_{1-x}Ca_xSi_2$ and $Ba_{1-x}Sr_xSi_2$ as a function of V/V_0. The calculated ΔE_g values of $Ba_7Ca_1Si_{46}$ and $Ba_7Sr_1Si_{46}$ are larger than those of $BaSi_2$ at all V/V_0 values, suggesting that the substitution of Ba atoms by Sr and Ca increases ΔE_g value when the unit cell volume remains the same after the substitution. The calculated ΔE_g values of $BaSi_2$, $Ba_7Ca_1Si_{46}$, and $Ba_7Sr_1Si_{46}$ decrease with decreasing V/V_0. The calculated ΔE_g value of $Ba_7Sr_1Si_{46}$ at $V/V_0 = 0.988$ agrees well with the experimental ΔE_g value of $Ba_{1-x}Sr_xSi_2$ with $x = 0.10$. Thus, the volume reduction due to Sr substitution is a main reason for decrease of band gap in $Ba_{1-x}Sr_xSi_2$. These results suggest that both substitution at $V = V_0$ and volume reduction are required to explain the experimental E_g value of $Ba_{1-x}Sr_xSi_2$. The decrease in E_g in $Ba_{1-x}Ca_xSi_2$ can also be explained by a combination of substitution and volume reduction effects qualitatively. However, the magnitude of experimental ΔE_g value of $Ba_{1-x}Ca_xSi_2$ with $x = 0.062$ (0.065 eV) is larger than that of calculated ΔE_g value of $Ba_7Ca_1Si_{46}$ at $V/V_0 = 0.982$ (0.008 eV). This indicates that considering the additional effect along with the substitution and volume reduction effects, such as the effect of defects introduction, is essential to more precisely explain the E_g value of $Ba_{1-x}Ca_xSi_2$.

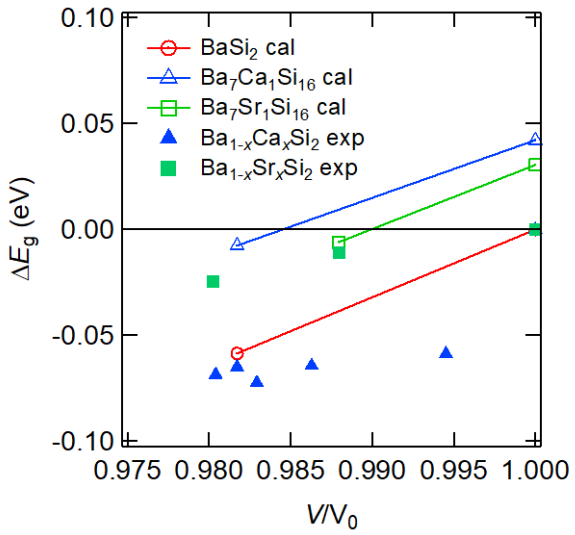

Fig. 7. Difference in E_g between substituted $BaSi_2$ and $BaSi_2$: $\Delta E_g = E_g(V/V_0) - E_{g0}$ as a function of V/V_0, where E_{g0} is the band gap of $BaSi_2$ at $V/V_0 = 1.00$. Solid and empty symbols represent the experimental and computational data, respectively.

4. Conclusion

The effects of substituting Ba with Ca atoms on the crystal structure and band gap (E_g)of $BaSi_2$ were investigated both experimentally and computationally. The solid-solution limit of the Ca atoms in $BaSi_2$ was approximately 2.3 at.%. Single-crystal XRD measurements of $Ba_{1-x}Ca_xSi_2$ ($0.025 \leq x \leq 0.072$) revealed that the unit cell volume decreases with x, and the Ba atoms at the A1 crystallographic site are preferentially substituted by Ca atoms. Diffuse reflectance spectroscopy results revealed that E_g decreases with x (1.24 eV at $x = 0$ and 1.17 eV at $x = 0.072$). The decreases in the lattice parameters, unit cell volume, and E_g in $Ba_{1-x}Ca_xSi_2$ were larger than those in $Ba_{1-x}Sr_xSi_2$ for a given substitution element content. The band gap calculations demonstrate that $Ba_{1-x}Ca_xSi_2$ is an indirect band gap semiconductor with VBM at a k-point between Γ and Y points and CBM at the T point; the same features were observed for $BaSi_2$ as well. The decrease in E_g by substitution observed experimentally can be explained qualitatively by a combination of substitution at $V=V_0$ and volume reduction. Volume reduction due to Ca substitution is mainly responsible for decrease of E_g in $Ba_{1-x}Ca_xSi_2$. To discuss the decrease in E_g by Ca substitution, considering additional effects such as defect introduction is essential. Practically, Ca substitution would be more effective for band gap tuning of $BaSi_2$ because it can decrease the E_g value with a smaller lattice deformation than Sr substitution. These results will be significant as a basic knowledge for band gap tuning in fabricating $BaSi_2$-based solar cell.

Declaration of competing interest

The authors declare that they have no known competing financial interests or personal relationships that could have appeared to influence the work reported in this paper.

CRediT Authorship contribution Statements

M. Imai: Conceptualization, Supervision, Project administration, Funding acquisitions, Resources, Investigation, Formal analysis, Validation, Data Curation, Visualization, Writing - Original draft, Writing – Review & editing.

Y. Matsushita: Investigation, Formal analysis, Writing – Review & editing.

Funding

This study was partially supported by Grants-in-Aid for Scientific Research (KAKENHI)

[grant numbers JP19H05819, JP22H00268] from the Japan Society for the Promotion of Science (JSPS).

Acknowledgments
The authors thank Mitsuaki Nishio of the National Institute for Materials Science (NIMS) for the EPMA and Masahiko Kawasaki of NIMS for sealing the samples in quartz tubes.

References

[1] Nakamura, T. Suemasu, K. Takakura, F. Hasegawa, A. Wakahara, M. Imai, Investigation of the energy band structure of orthorhombic $BaSi_2$ by optical and electrical measurements and theoretical calculations, Appl. Phys. Lett. 81 (2002) 1032–1034. https://doi.org/10.1063/1.1498865.

[2] T. Suemasu, Exploring the possibility of semiconducting $BaSi_2$ for thin-film solar cell applications, Jpn. J. Appl. Phys. 54 (2015) 07ja01 and references therein. https://doi.org/10.7567/jjap.54.07ja01.

[3] T. Suemasu, N. Usami, Exploring the potential of semiconducting $BaSi_2$ for thin-film solar cell applications, J. Phys. D Appl. Phys. 50 (2017) 023001 and references therein. https://doi.org/10.1088/1361-6463/50/2/023001.

[4] T. Suemasu, D.B. Migas, Recent progress toward realization of high-efficiency $BaSi_2$ solar cells: thin-film deposition techniques and passivation of defects, Phys. Status Solidi A 219 (2022) 2100593. https://doi.org/10.1002/pssa.202100593.

[5] M. Kumar, N. Umezawa, W. Zhou, M. Imai, Barium disilicide as a promising thin-film photovoltaic absorber: structural, electronic and defects properties, J. Mater. Chem. A 5 (2017) 25293–25302. https://doi.org/10.1039/C7TA08312B.

[6] M. Kumar, N. Umezawa, M. Imai, Recent advances in computational studies of thin-film solar cell material $BaSi_2$, Jpn. J. Appl. Phys. 59 (2020) SF0803. https://doi.org/10.35848/1347-4065/ab6b82.

[7] D. Tsukahara, S. Yachi, H. Takeuchi, R. Takabe, W.J. Du, M. Baba, Y.P. Li, K. Toko, N. Usami, T. Suemasu, p-$BaSi_2$/n-Si heterojunction solar cells with conversion efficiency reaching 9.0%, Appl. Phys. Lett. 108 (2016) 152101. https://doi.org/10.1063/1.4945725.

[8] S. Yachi, R. Takabe, H. Takeuchi, K. Toko, T. Suemasu, Effect of amorphous Si capping layer on the hole transport properties of $BaSi_2$ and improved conversion efficiency approaching 10% in p-$BaSi_2$/n-Si solar cells, Appl. Phys. Lett. 109 (2016) 072103. https://doi.org/10.1063/1.4961309.

[9] K. Morita, M. Kobayashi, T. Suemasu, Optical absorption edge of ternary semiconducting silicide $Ba_{1-x}Sr_xSi_2$, Jpn. J. Appl. Phys. Part 2 45 (2006) L390–L392. https://doi.org/10.1143/JJAP.45.L390.

[10] Y. Imai, A. Watanabe, Consideration of the band-gap tunability of $BaSi_2$ by alloying with Ca or Sr based on the electronic structure calculations, Thin Solid Films 515 (2007) 8219–8225. https://doi.org/10.1016/j.tsf.2007.02.060.

[11] M. Imai, M. Kumar, Y. Matsushita, N. Umezawa, Crystal structure and electronic properties of Sr-substituted barium disilicide $Ba_{1-x}Sr_xSi_2$ for solar cells: computational

and experimental studies, Acta Mater. 148 (2018) 492–498. https://doi.org/10.1016/j.actamat.2018.02.010.
[12] H. Schäfer, K.H. Janzon, A. Weiss, $BaSi_2$, a phase with discrete Si_4 tetrahedra, Angew. Chem. Int. Ed. 2 (1963) 393–394. https://doi.org/10.1002/ange.19630751010.
[13] B. Eisenmann, C. Riekel, H. Schafer, A. Weiss, Ternary disilicides of alkali-earth metals, Z. Anorg. Allg. Chem. 372 (1970) 325–331. https://doi.org/10.1002/zaac.19703720309.
[14] T. Suemasu, K. Hara, H. Udono, M. Imai, Silicon meets group-II metals in energy and electronic applications—How to handle reactive sources for high-quality films and bulk crystals, J. Appl. Phys. 131 (2022) 191101. https://doi.org/10.1063/5.0092080.
[15] CrystalClear, Rigaku Co., Tokyo, Japan, 1997–2022.
[16] G.M. Sheldrick, A short history of SHELX, Acta Crystallogr. A64 (2008) 112–122. https://doi.org/10.1107/S0108767307043930.
[17] W.W. Wendlandt, H.G. Harry, Reflectance Spectroscopy, Interscience Publishers, New York, 1966.
[18] J.P. Perdew, K. Burke, M. Ernzerhof, Generalized gradient approximation made simple, Phys. Rev. Lett. 77 (1996) 3865–3868. https://doi.org/10.1103/PhysRevLett.77.3865.
[19] Advance/PHASE, AdvanceSoft Co., Tokyo, Japan, 2005–2022.
[20] M. Imai, A. Sato, T. Kimura, T. Aoyagi, Basic properties of $Sr_{1-x}Ba_xSi_2$, Thin Solid Films 519 (2011) 8496–8500. https://doi.org/10.1016/j.tsf.2011.05.040.
[21] M. Imai, M. Kumar, N. Umezawa, Electronic states of Zintl-phase solar-cell material $BaSi_2$, Scripta Mater 172 (2019) 43. https://doi.org/10.1016/j.scriptamat.2019.07.004.
[22] M. Imai, A. Sato, Y. Matsushita, Effect of temperature on the crystal structure of $BaSi_2$, Phys. B 572 (2019) 302–307. https://doi.org/ /10.1016/j.physb.2019.06.018.
[23] S.P. Tandon, J.P. Gupta, Measurement of forbidden energy gap of semiconductors by diffuse reflectance technique, Phys. Status Solidi 38 (1970) 363–367. https://doi.org/10.1002/pssb.19700380136.
[24] D.B. Migas, V.L. Shaposhnikov, V.E. Borisenko, Isostructural $BaSi_2$, $BaGe_2$ and $SrGe_2$: electronic and optical properties, Phys. Status Solidi B 244 (2007) 2611–2618. https://doi.org/10.1002/pssb.200642556.